Original Research
Date

Frequency-domain Optimal Viscous Damper Placement Using Lower-bound Transfer Function and Multi-modal Adaptability

Hiroki Akehashi[1], **Izuru Takewaki**[1]*

[1]Department of Architecture and Architectural Engineering, Graduate School of Engineering, Kyoto University, Kyotodaigaku-Katsura, Nishikyo, Kyoto 615-8540, Japan

*** Correspondence:** Izuru Takewaki; E-mail takewaki@archi.kyoto-u.ac.jp

Abstract

A new concept of a 'lower-bound transfer function (LBTF)' and a new frequency-domain optimal damper design method are presented. LBTF expresses an ideal performance for response control in the frequency domain under a constant sum of added damping coefficients (or the total cost of dampers). The effectiveness of the damper design for each mode can be captured visually through plotting the transfer function amplitudes of the model and the LBTF. An efficient generation method of LBTFs is also proposed. The proposed design method provides designs with multi-modal adaptability (effective for multi-modes). It does not require much computational load to implement the method since the optimization is conducted in the frequency domain and the first-order or second-order sensitivities of the objective function can be derived analytically. The proposed design and the fundamental mode optimal damper placement are compared for shear-mass systems and moment-resisting frames through the transfer functions and the Incremental Dynamic Analysis (IDA). It is demonstrated that the proposed designs effectively reduce the floor acceleration responses and the elastic deformation responses. Moreover, it is shown that the proposed designs can effectively reduce the elastic-plastic responses although the optimization is conducted for linear elastic models.

Keywords: Earthquake response, Viscous damper, Optimization, Frequency-domain optimization, Lower-bound transfer function, Multi-modal adaptability.

1. Introduction

Researches on passive control of structural systems have been widely investigated so far[1-4]. Zhang and Soong[5] and Garcia[6] proposed sequential procedures for damper placement. Takewaki[7] applied an incremental inverse problem approach to the simultaneous optimization of story stiffness and viscous damping. Trombetti and Silvestri[8] demonstrated the effectiveness of mass-proportional damping systems and investigated the applicability of the systems to realistic building models. Lavan and Levy[9] effectively used an active earthquake to save the computational load for damper optimization under multiple ground motions. Cimellaro and Retamales[10] and Silvestri et al.[11] used design earthquake response spectrums to obtain preliminary designs of structures and dampers. Lavan and Dargush[12] treated a multi-objective optimization problem for simultaneous placement of viscous, viscoelastic and hysteretic dampers. Apostolakis and Dargush[13] proposed a design framework for hysteretic dampers. Yamamoto et al.[14] conducted H^{∞} optimization of the transfer function of interstory drifts. Whittle et al.[15] compared several optimization techniques in view of reduction performances in peak responses, usability and computational load. Sonmez et al.[16] applied an artificial bee colony algorithm to damper optimization. Martínez et al.[17] treated an optimization problem of hysteretic damper placement in the frequency domain by using the stochastic equivalent linearization technique. Pollini et al.[18] tackled a simultaneous optimization of nonlinear fluid viscous dampers and their supporting braces. Cetin et al.[19] dealt with an optimization problem of damper placement under the critical excitation. De Domenico and Ricciardi[20] incorporated a nonlinear response estimation method of fluid viscous dampers using a non-Gaussian stochastic linearization formulation into an optimization procedure. Aydin et al.[21] investigated the effect of soil-structure interaction on the optimal damper placement. Apostolakis[22] introduced a multiscale approach to a genetic algorithm-based optimization of friction damper placement for 3D building structures. Marzok and Lavan[23] tackled an optimal design problem for multiple-rocking systems.

In almost all of the above-mentioned researches, elastic structural frames were treated. However, it is important to take the elastic-plastic responses of the frames into account when structural optimization is conducted because recently observed ground motions greatly exceed the level of the code-specified ground motions. There have been a few researches which take into account the elastic-plastic responses of frames in the damper optimization problems[24-27]. Attard[28] applied a gradient-based method for optimal viscous damper placement for nonlinear shear building structures. Akehashi and Takewaki[29] developed a consecutive design generation method to obtain damper designs which are effective for multi-level ground motions.

As stated above, the optimal damper placement methods can be classified in view of response evaluation as follows: (i) response spectrum-based methods, (ii) time-domain optimization methods, (iii) frequency-domain optimization methods. Especially, as for the frequency-domain optimization methods, Takewaki[30] treated an optimal viscous damper placement problem for a shear building structure with respect to the sum of amplitudes of interstory drifts at the fundamental natural frequency of the structure under a constant sum of added damping coefficients. Aydin et al.[31] extended this approach to the transfer function amplitude in terms of the base shear force at the fundamental natural frequency. When sufficient amount of added damping is given, this method provides a design with high safety margin since the structure performs elastically and the higher-mode responses hardly contribute to the displacement responses. Akehashi and Takewaki[32] extended the concept developed by Takewaki[30] into higher modes and proposed the concept of 'the *n*-th mode optimal damper placement'. At the same, it is also important to reduce floor acceleration responses in view of the damage of nonstructural components and facilities[33-36]. Moreover, in the case of high-rise buildings, the predominant periods of ground motions may coincide with the second, or third natural periods of the buildings. Therefore, both of the fundamental natural mode and the higher modes should be taken into account for damper designs.

It is widely known that the transfer function-based design methods directly treat the system characteristics and need low computational load. However, most of recent researches on the optimal damper placement deal with time-domain optimization methods. This is because nonlinear responses of dampers and structures need to be treated and the performances of computers have been increasing. However, since the transfer function-based method still has an advantageous feature, an alternative optimization method using transfer functions is newly proposed in this paper. The purpose of the proposed method is to obtain designs which are effective for multi modes. Such designs will effectively reduce both elastic deformation responses and floor acceleration responses. Moreover, such designs may also be safe for large-amplitude ground motions. The amplification of the higher-mode effect due to the elastic-plastic responses is unpredictable because it strongly depends on the nature of input ground motions and that of the structural design. However, if a design is not effective for the specified modes, the corresponding modes are largely amplified due to the elastic-plastic responses. Therefore, if an optimal design method using transfer functions for linear elastic models can realize designs which are effective for multi modes, such designs are expected to effectively reduce the elastic-plastic responses.

In this paper, a new concept of 'lower-bound transfer function (LBTF)' and a new frequency-domain optimal damper design method are presented. LBTF expresses an ideal performance for response control in the frequency domain under the constant sum of added damping coefficients (or the total cost of dampers). The effectiveness of a damper design for each mode can be captured visually through plotting the transfer function amplitudes of the model and LBTF. An efficient generation method of LBTFs is also proposed. The proposed design method provides designs with multi-modal adaptability (effective for multi-modes). It does not require much computational load to implement the method since the optimization is conducted in the frequency domain and the first-order or second-order sensitivities of the objective function can be derived analytically. The proposed design and the optimal damper placement for the fundamental mode are compared for shear-mass systems and moment-resisting frames through the transfer functions and incremental dynamic analysis (IDA)[37]. It is demonstrated that the proposed designs effectively reduce the floor acceleration responses, the elastic deformation responses. Moreover, it is shown that the proposed design can effectively reduce the elastic-plastic responses although the optimization is conducted for linear elastic models.

2. Optimization problem

Takewaki[30] treated an optimal viscous damper placement problem for a shear building structure with respect to the sum of the interstory drift amplitudes at the fundamental natural frequency of the structure under a constant sum of added damping coefficients. Since the sum of added damping coefficients is almost proportional to the total cost of added dampers, the constraint on the sum of added damping coefficients is almost equivalent to the constraint on the total cost of added dampers. When a sufficient amount of added damping is given, this method provides a design with high safety since the structure performs elastically and the higher-mode responses hardly contribute to the displacement responses. Akehashi and Takewaki[32] extended the concept developed by Takewaki[30] into higher modes and proposed the concept of 'the *n*-th mode optimal damper placement'. Both the fundamental natural mode and the higher modes should be taken into account for damper designs because the floor acceleration responses are directly related to the damage of the nonstructural components and facilities. Especially in the case of high-rise buildings, the predominant period of ground accelerations may coincide with the second or third natural period of the buildings. Moreover, in the case that the ground motion exceeds the level of the ground motion for the damper design, the structure performs inelastically and the higher-mode responses are amplified.

In Section 2.1, the problems which Takewaki[30] and Akehashi and Takewaki[32] treated are explained briefly. In Section 2.2, a new concept of 'lower-bound transfer function (LBTF)' is proposed for the visualization of the effectiveness of a damper design for each mode and its generation method is explained. Figure 1a illustrates the concept of LBTF and the 1-3th mode optimal damper placements. LBTF expresses an ideal performance for response control in the frequency domain under a constant sum of added damping coefficients. For examples, when a design is effective for the fundamental natural mode but not effective for the 2, 3th modes, the amplitudes of the transfer function is plotted away from the LBTF near the 2, 3th natural frequencies. On the other hand, when a design is effective for multi modes, the transfer function is plotted near LBTF for a broader frequency range. Figure 1b shows an example of such designs. In Section 2.3, an optimization problem to obtain designs with multi-modal adaptability is formulated and its solution algorithm is presented.

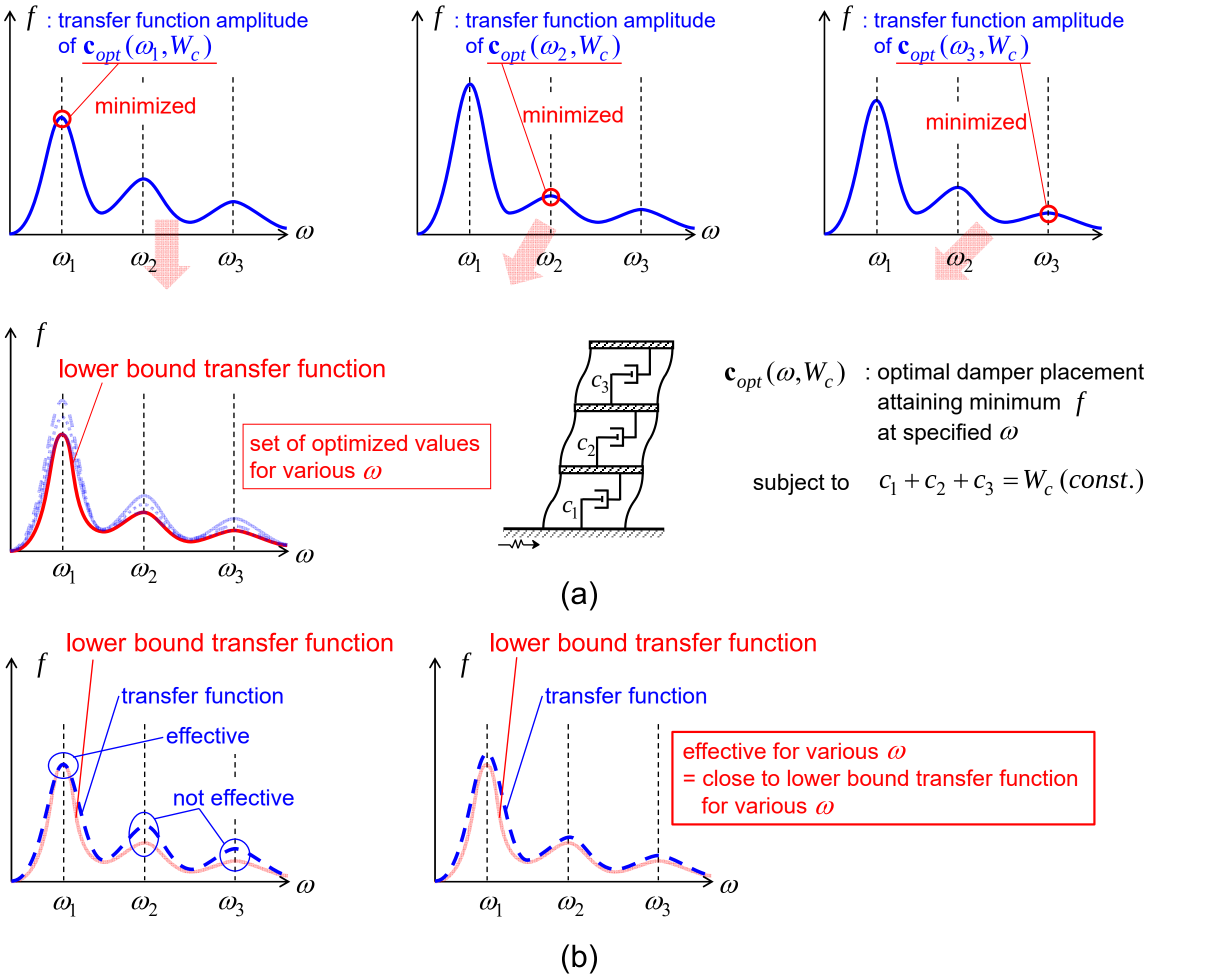

Fig. 1 Concept of lower-bound transfer function (LBTF) and response control performance in frequency domain, (a) LBTF, (b) response control performance in frequency domain.

2.1 Optimal damper placement with respect to sum of transfer function amplitudes at natural circular frequency

Consider an N-story shear-mass system. Let $\mathbf{c} = (c_1, ..., c_N)^T$ and $\delta_i(\omega)$ denote the added damping coefficient vector and the transfer function of the i-th interstory drift, and $\boldsymbol{\delta} = (\delta_1, ..., \delta_N)^T$. The problem which Takewaki[30] and Akehashi and Takewaki[32] treated is described as follows.

[Problem]

$$\begin{aligned}&\textit{Find}\ \mathbf{c}=(c_1,...,c_N)^T\\&\textit{so as to minimize}\ f=\sum_{i=1}^{N}|\delta_i(\mathbf{c},\hat{\omega})|\qquad,\\&\textit{subjected to}\ \begin{cases}\mathbf{c}^T\cdot\mathbf{1}=W_c & (const.)\\ 0\le c_i\le c_i^U & (\text{for}\ i=1,...,N)\end{cases}\end{aligned}\tag{1}$$

where $W_c, c_i^U, \mathbf{1}$ denote the sum of added damping coefficients, the upper bound of the damping coefficient added at the *i*-th story and the vector with 1 at every component. Takewaki[30] adopted the undamped fundamental natural circular frequency ω_1 for the value of $\hat{\omega}$ and Akehashi and Takewaki[32] adopted the undamped 1-3th natural circular frequencies $\omega_1, \omega_2, \omega_3$. It is noted that $|\delta_i(\omega)|$ corresponds to the *i*-th steady-state intersroty drift under the harmonic excitation with single frequency $\hat{\omega}$.

When the constraints on the upper bound of c_i are not included in the problem, the Lagrangian function L for the problem is expressed by

$$L=f+\lambda_c(c_1+...+c_N-W_c)+\{\mu_1(-c_1)+...+\mu_N(-c_N)\}\ ,\tag{2}$$

where λ_c, μ_i are the Lagrange multipliers. From Eq. (2), the optimality criteria for the problem can be obtained by

$$(\partial f/\partial c_i)+\lambda_c-\mu_i=0\qquad (i=1,...,N),\tag{3}$$

$$c_1+...+c_N=W_c,\tag{4}$$

$$c_i\ge 0, \mu_i\ge 0, \mu_i c_i=0\qquad (i=1,...,N)\tag{5}$$

Takewaki[30] developed an optimality criterion-based approach for the solution algorithm of the problem. Hereafter, the optimal design for the problem is designated by $\mathbf{c}_{opt}(\omega,W_c)$ in place of $\mathbf{c}_{opt}(\hat{\omega},W_c)$ because the specified circular frequency $\hat{\omega}$ is extended to all the frequency ω.

2.2 Importance of lower-bound transfer function (LBTF) and its generation method

Let us define LBTF $f_{lb}(\omega,W_c)$ as follows.

$$f_{lb}(\omega,W_c)=f(\mathbf{c}_{opt}(\omega,W_c),\omega)\tag{6}$$

Since $\mathbf{c}_{opt}(\omega,W_c)$ is the optimal design for minimizing the sum of the transfer function amplitudes of the interstory drifts, $f_{lb}(\omega,W_c)$ is the lower bound of $f(\mathbf{c},\omega)$ for any damper designs with $c_1+...+c_N=W_c$. In other words, the sum of the transfer function amplitudes of $\mathbf{c}_{opt}(\omega,W_c)$ is tangent to LBTF $f_{lb}(\omega,W_c)$ only at the point where ω coincides, the sum of the transfer function amplitudes runs above $f_{lb}(\omega,W_c)$ at any other points. Therefore, $f_{lb}(\omega,W_c)$ expresses an ideal performance for response control in the frequency domain under the constraint $c_1+...+c_N=W_c$.

The effectiveness of the damper design in the frequency domain should be judged through the comparison between the sum of the transfer function amplitudes and the corresponding LBTF. This is because the amount of W_c (or the total cost of dampers) greatly affects how small the amplitudes become. When the transfer function is plotted near LBTF for a broader frequency range, it indicates that the design is effective for multi modes.

It is inefficient to repeat the optimization procedure and find $\mathbf{c}_{opt}(\omega, W_c)$ as many as frequencies for obtaining LBTF. An efficient generation method of LBTF is explained below.
Assume that $\mathbf{c}_{opt}(\omega, W_c)$, which satisfies Eqs. (3)-(5), has been obtained. Since $\mathbf{c}_{opt}(\omega+\Delta\omega, W_c)$ must satisfy Eqs. (3), (4), the following equations must also be satisfied.

$$\begin{aligned} g_i &= \left\{\frac{\partial f}{\partial c_i} + \sum_{j=1}^{N} \frac{\partial^2 f}{\partial c_j \partial c_i}\Delta c_j + \frac{\partial^2 f}{\partial \omega \partial c_i}\Delta\omega\right\} + \{\lambda_c + \Delta\lambda_c\} - \{\mu_i + \Delta\mu_i\} \\ &= \sum_{j=1}^{N} \frac{\partial^2 f}{\partial c_j \partial c_i}\Delta c_j + \frac{\partial^2 f}{\partial \omega \partial c_i}\Delta\omega + \Delta\lambda_c - \Delta\mu_i = 0 \end{aligned} \quad (i = 1, ..., N), \quad (7)$$

$$\Delta c_1 + ... + \Delta c_N = 0, \quad (8)$$

Eq. (7) corresponds to Eq. (3) and Eq. (8) corresponds to Eq. (4). Then g_i' is introduced to delete $\Delta\lambda_c$ from Eq. (7).

$$\begin{aligned} g_i' &= g_1 - g_i \\ &= \sum_{j=1}^{N}\left(\frac{\partial^2 f}{\partial c_j \partial c_1} - \frac{\partial^2 f}{\partial c_j \partial c_i}\right)\Delta c_j + \left(\frac{\partial^2 f}{\partial \omega \partial c_1} - \frac{\partial^2 f}{\partial \omega \partial c_i}\right)\Delta\omega - (\Delta\mu_1 - \Delta\mu_i) \\ &= 0 \end{aligned} \quad (i = 2, ..., N), \quad (9)$$

Since $g_1 = ... = g_N = 0$, $g_2' = ... = g_N' = 0$ is required. The simultaneous formulation of $(g_2', ..., g_N')^T = \mathbf{0}$ and Eq. (8) leads to

$$\begin{pmatrix} \frac{\partial^2 f}{\partial^2 c_1^2} - \frac{\partial^2 f}{\partial c_1 \partial c_2} & \cdots & \frac{\partial^2 f}{\partial c_N \partial c_1} - \frac{\partial^2 f}{\partial c_N \partial c_2} \\ \vdots & \ddots & \vdots \\ \frac{\partial^2 f}{\partial^2 c_1^2} - \frac{\partial^2 f}{\partial c_1 \partial c_N} & \cdots & \frac{\partial^2 f}{\partial c_N \partial c_1} - \frac{\partial^2 f}{\partial c_N^2} \\ 1 & \cdots & 1 \end{pmatrix} \begin{pmatrix} \Delta c_1 \\ \vdots \\ \Delta c_N \end{pmatrix} = -\Delta\omega \begin{pmatrix} \frac{\partial^2 f}{\partial \omega \partial c_1} - \frac{\partial^2 f}{\partial \omega \partial c_2} \\ \vdots \\ \frac{\partial^2 f}{\partial \omega \partial c_1} - \frac{\partial^2 f}{\partial \omega \partial c_N} \\ 0 \end{pmatrix} + \begin{pmatrix} \Delta\mu_1 - \Delta\mu_2 \\ \vdots \\ \Delta\mu_1 - \Delta\mu_N \\ 0 \end{pmatrix} \quad (10)$$

By solving Eq. (10), $\mathbf{c}_{opt}(\omega+\Delta\omega, W_c) = \mathbf{c}_{opt}(\omega, W_c) + \Delta\mathbf{c}$ can be obtained. It is noted that $\Delta\mu_i$ is set to zero when c_i is large enough. In the case that c_i is nearly zero or equal to zero, $c_i + \Delta c_i$ is calculated with $\Delta\mu_i = 0$ first. If $c_i + \Delta c_i < 0$, $\Delta\mu_i$ is updated so that $c_i + \Delta c_i$ becomes zero. Figure 2 represents the relation between c_i and μ_i. The generation method of LBTF may be described as follows.

[Algorithm]

Step 1 Set the search range as $\omega^L \le \omega \le \omega^U$. Put $i_\omega \to 1$.

Step 2 Solve the problem expressed by Eq. (1) and obtain the optimal damper placement $\mathbf{c}_{opt}(\omega_{i_\omega}, W_c)$, where ω_{i_ω} is the i_ω-th undamped fundamental natural circular frequency.

Step 3 Set $\mathbf{c}_{opt}(\omega_{i_\omega}, W_c)$ as an initial design, then solve Eq. (10) repeatedly to obtain the optimal designs and the corresponding transfer functions in the range of $\omega_{i_\omega} \le \omega \le \min\{\omega^U, \omega_{i_\omega+1}\}$.

Step 4 Set $\mathbf{c}_{opt}(\omega_{i_\omega}, W_c)$ as an initial design, then solve Eq. (10) repeatedly to obtain the optimal designs and the corresponding transfer functions in the range of $\max\{\omega^L, \omega_{i_\omega-1}\} \le \omega \le \omega_{i_\omega}$. When $i_\omega = 1$, the range is replaced with $\omega^L \le \omega \le \omega_{i_\omega}$.

Step 5 If $i_\omega = n_\omega$, go to Step 6. Otherwise, put $i_\omega \to i_\omega + 1$ and return to Step 2.

Step 6 Select the design which exhibits the minimum value of f at each ω, then finalize the process.

Figure 3 shows the search order of LBTF. It is noted that the added dampers can decrease the transfer function amplitudes near the natural circular frequencies. However, the added dampers hardly affect the transfer function amplitudes in the intermediate range between two adjacent natural circular frequencies $\omega_{i_\omega}, \omega_{i_\omega+1}$. Although the search with $\mathbf{c}_{opt}(\omega_{i_\omega}, W_c)$ as an initial design works well near ω_{i_ω}, it may lead to local optimal solutions in the intermediate range between $\omega_{i_\omega}, \omega_{i_\omega+1}$, and the solutions obtained near $\omega_{i_\omega+1}$ may not be global optimum. To avoid such unsuccessful search near $\omega_{i_\omega+1}$, the initial design is changed n_ω times in the proposed method. As a result, the search is carried out multiple times in the specific frequency range. Therefore, the design which exhibits the minimum value of f is selected in the Step 6.

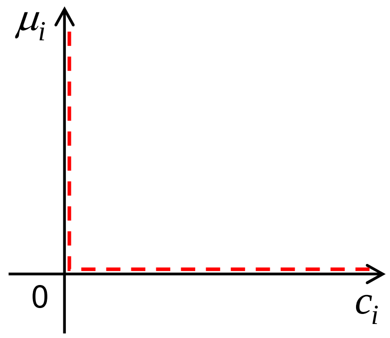

Fig. 2 Relation between added damping coefficient c_i in *i*-th story and Lagrange multiplier μ_i corresponding to constraint $c_i \geq 0$.

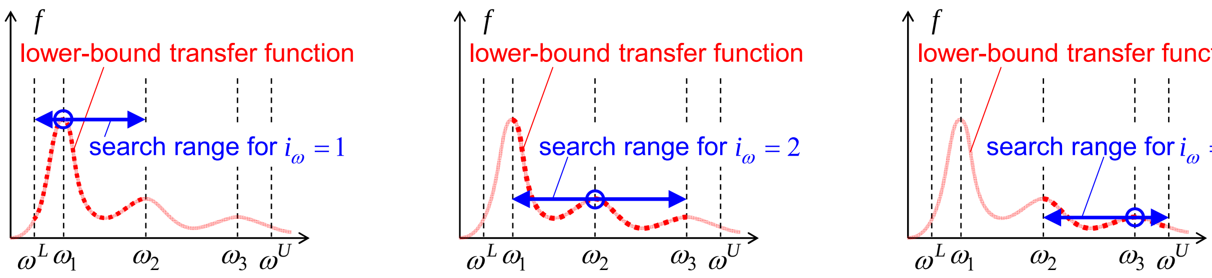

Fig. 3 Search order of LBTF.

2.3 Design problem of damper placement effective for multi modes and its solution algorithm

When the transfer function is close to the LBTF for a broader frequency range, such design has multi-modal adaptability. Consider the following problem to systematically obtain damper designs with multi-modal adaptability.

[Problem]

$$\begin{aligned} & \textit{Find}\ \mathbf{c} = (c_1, \ldots, c_N)^T \\ & \textit{so as to minimize}\ f_{tf} = \sum_{j=1}^{N_\omega} f(\mathbf{c}, \omega^L + (j-1)\Delta\omega)\Delta\omega \\ & \qquad\qquad = \sum_{j=1}^{N_\omega}\sum_{i=1}^{N} |\delta_i(\mathbf{c}, \omega^L + (j-1)\Delta\omega)|\Delta\omega, \\ & \textit{subjected to} \begin{cases} \mathbf{c}^T \cdot \mathbf{1} = W_c & (\textit{const.}) \\ 0 \leq c_i \leq c_i^U & (\text{for } i = 1, \ldots, N) \end{cases} \end{aligned} \tag{11}$$

The objective function f_{tf} for an integrated transfer function amplitude is an approximation of the integration of f by the rectangle rule (Figure 4a). It is noted that it does not require much computational load to solve this problem since the optimization is conducted in frequency domain and the first-order or second-order sensitivities of the objective function can be derived analytically (the first-order or second-order sensitivities of f have been derived by Takewaki[30]). This problem can be solved by the algorithm proposed by Takewaki[30]. The algorithm is briefly explained here, although some expressions of the formulations are rewritten in a simpler manner.

The first-order sensitivity of f_{tf} is approximated by the following equation.

$$\left.\frac{\partial f_{tf}}{\partial c_i}\right|_{\mathbf{c}+\Delta\mathbf{c}} \cong \left.\frac{\partial f_{tf}}{\partial c_i}\right|_{\mathbf{c}} + \sum_{j=1}^{N} \left.\frac{\partial^2 f_{tf}}{\partial c_j \partial c_i}\right|_{\mathbf{c}} \Delta c_j \qquad (i = 1, \ldots, N) \qquad (12)$$

Since the first-order sensitivity of f_{tf} at the optimal solution is parallel to the normal vector of the hyperplane $c_1 + \ldots + c_N = W_c$ (Figure 4b), the following equation is obtained.

$$\partial f_{tf} / \partial c_1 = \ldots = \partial f_{tf} / \partial c_N \qquad (13)$$

The simultaneous formulation of $(\partial f_{tf} / \partial c_1)_{|\mathbf{c}+\Delta\mathbf{c}} \mathbf{1} - \{(\partial f_{tf} / \partial c_2)_{|\mathbf{c}+\Delta\mathbf{c}}, \ldots, (\partial f_{tf} / \partial c_N)_{|\mathbf{c}+\Delta\mathbf{c}}\}^T = \mathbf{0}$ and $\Delta c_1 + \ldots + \Delta c_N = 0$ leads to

$$\begin{pmatrix} \dfrac{\partial^2 f_{tf}}{\partial^2 c_1^2} - \dfrac{\partial^2 f_{tf}}{\partial c_1 \partial c_2} & \cdots & \dfrac{\partial^2 f_{tf}}{\partial c_N \partial c_1} - \dfrac{\partial^2 f_{tf}}{\partial c_N \partial c_2} \\ \vdots & & \vdots \\ \dfrac{\partial^2 f_{tf}}{\partial^2 c_1^2} - \dfrac{\partial^2 f_{tf}}{\partial c_1 \partial c_N} & \cdots & \dfrac{\partial^2 f_{tf}}{\partial c_N \partial c_1} - \dfrac{\partial^2 f_{tf}}{\partial c_N^2} \\ 1 & \cdots & 1 \end{pmatrix} \begin{pmatrix} \Delta c_1 \\ \vdots \\ \Delta c_N \end{pmatrix} = - \begin{pmatrix} \dfrac{\partial f_{tf}}{\partial c_1} - \dfrac{\partial f_{tf}}{\partial c_2} \\ \vdots \\ \dfrac{\partial f_{tf}}{\partial c_1} - \dfrac{\partial f_{tf}}{\partial c_N} \\ 0 \end{pmatrix} \qquad (14)$$

By solving the Eq. (14) repeatedly and updating $\mathbf{c} \to \mathbf{c} + \alpha \Delta \mathbf{c}$ (α : small positive number), the optimal solution is obtained. It is noted that, when $c_j = 0$ and $c_j + \alpha \Delta c_j < 0$, all the elements regarding c_j are deleted from Eq. (14) and $\Delta \mathbf{c}$ is modified. If $c_1 = 0$, Eq. (14) is replaced with the simultaneous formulation of $(\partial f_{tf} / \partial c_2)_{|\mathbf{c}+\Delta\mathbf{c}} \mathbf{1} - \{(\partial f_{tf} / \partial c_3)_{|\mathbf{c}+\Delta\mathbf{c}}, \ldots, (\partial f_{tf} / \partial c_N)_{|\mathbf{c}+\Delta\mathbf{c}}\}^T = \mathbf{0}$ and $\Delta c_2 + \ldots + \Delta c_N = 0$. The optimal design for the problem is designated by $\mathbf{c}_{tf}$ (optimized for <u>transfer function</u>) hereafter.

It should be noted that the H^∞ optimization is one of the famous control theories in the frequency domain. The H^∞ norm of the transfer function of the interstory drifts is expressed by $\|\boldsymbol{\delta}(\omega)\|_\infty = \sup_{\omega} \left\{ \sqrt{\sum_{i=1}^{N} |\delta_i(\omega)|^2} \right\}$. The components of $\boldsymbol{\delta}(\omega)$ near the fundamental natural frequency and those of $\sqrt{\sum_{i=1}^{N} |\delta_i(\omega)|^2}$ are much larger than those in other range even if a sufficient amount of added damping is given. Therefore, the H^∞ optimization of $\boldsymbol{\delta}(\omega)$ may not be always effective for the higher modes. On the other hand, the proposed method aims at damper designs with multi-modal adaptability.

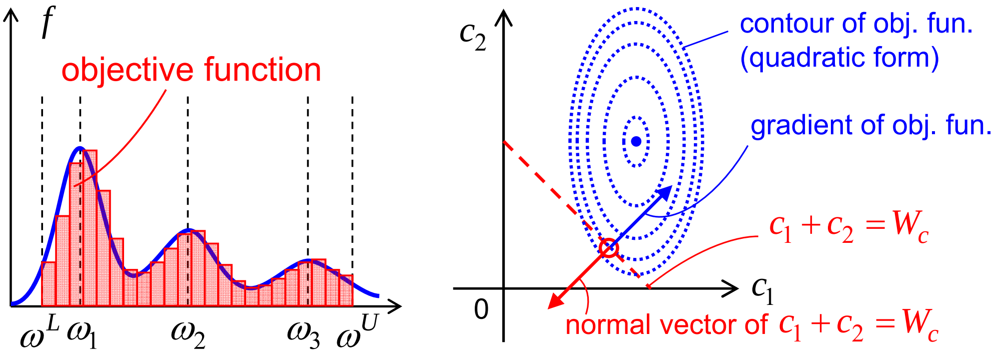

(a) (b)

Fig. 4 Overview of optimization problem, (a) objective function, (b) relation between gradient of objective function and normal vector of hyperplane $c_1 + ... + c_N = W_c$ (example for N=2).

The formulations in Section 2.1-2.3 are applicable to the optimal damper placement for moment-resisting frames by adding some modifications. Numerical examples for shear-mass systems are shown in Section 3, and numerical examples for moment-resisting frames are shown in Section 4.

3. Numerical examples for shear-mass system

In this section, $\mathbf{c}_{opt}(\omega_1)$ and $\mathbf{c}_{tf}$ for shear-mass systems are compared through the transfer functions and incremental dynamic analysis (IDA)[37]. It is demonstrated that $\mathbf{c}_{tf}$ is effective for the multi modes, although $\mathbf{c}_{opt}(\omega_1)$ is effective only for the fundamental natural mode and not effective for the higher modes. In addition, it is shown that $\mathbf{c}_{tf}$ effectively reduces the elastic-plastic responses although the optimization is conducted without considering the nonlinearity of the structures. $\mathbf{c}_{opt}(\omega_2), \mathbf{c}_{opt}(\omega_3), \mathbf{c}_{opt}(\omega_4)$ are shown in Appendix just for reference.

Consider two shear building models of 12 stories with different story stiffness distributions. Model 1 has a trapezoidal distribution of story stiffnesses ($k_1 / k_{12} = 2.5$). Model 2 has the uniform story stiffness distribution at every four stories (1-4, 5-8, 9-12: stiffness ratio is 2:1.5:1 from the bottom). The undamped fundamental natural period of these two models is 1.2[s] and the structural damping ratio is 0.01 (stiffness proportional type). All the floor masses have the same value ($m_i = 400 \times 10^3$ [kg]). The common story height is 4[m]. In the IDA analyses, the common yield interstory drift d_y is set to 4/150 [m]. The story shear-interstory drift relation obeys the elastic perfectly-plastic rule.

El Centro NS component during the Imperial Valley earthquake (1940) and Taft EW component during the Kern County earthquake (1952) are employed as representatives of ground motions of random nature. In addition, Rinaldi station fault-normal component during the Northridge earthquake

(1994) and Kobe University NS component during the Hyogoken-nanbu earthquake (1995) are employed as representatives of ground motions of pulse type. PGV (peak ground velocity) in the IDA analyses is increased from 0.2 [m/s] to 1.0 [m/s] by the increment 0.02 [m/s].

The sum of added damping coefficients is set to $W_c = 20\times10^7$ [Ns/ m] so that the fundamental-mode damping ratio by the dampers becomes about 0.10. $\omega^L = 0.9\omega_1, \omega^U = 1.1\omega_4, n_\omega = 4, N_\omega = 1000$ are employed for obtaining LBTF and $\mathbf{c}_{tf}$. The search range is set to be slightly wider than the range between ω_1 and ω_4 because the peaks of the transfer function amplitudes do not always coincide with the undamped natural frequencies. The initial damper design for the search of $\mathbf{c}_{opt}(\omega_1),...,\mathbf{c}_{opt}(\omega_4)$ is set to $(c_1 \cdots c_{12})^T = (W_c/12)\mathbf{1}[\mathrm{Ns/m}]$. $\mathbf{c}_{opt}(\omega_1)$ is employed as the initial design for the search of $\mathbf{c}_{tf}$.

Figures 5, 6 show the distributions of added damping coefficients of $\mathbf{c}_{opt}(\omega_1), \mathbf{c}_{tf}$, the normalized sum of the transfer function amplitudes of the interstory velocities and normalized LBTFs. The transfer function amplitudes of the interstory velocities are plotted for visibility in place of those of the interstory drifts. In addition, the transfer function amplitudes and LBTFs are normalized so that the maximum value of LBTFs becomes one. It can be observed that the added dampers are placed to the specified stories for $\mathbf{c}_{opt}(\omega_1)$, and the added dampers are placed to relatively many stories for $\mathbf{c}_{tf}$. Moreover, the transfer function amplitudes of $\mathbf{c}_{opt}(\omega_1)$ are away from LBTF near the higher-mode natural frequencies. However, the transfer function amplitudes are close to LBTF near ω_1. On the other hand, the transfer function amplitudes of $\mathbf{c}_{tf}$ are close to LBTF for a broader frequency range.

Figures 7-10 present the results of the IDA analyses. The distributions of the maximum interstory drifts and the distributions of the maximum floor accelerations are plotted for PGV = 0.2, 0.4, …, 1.0 [m/s]. It can be observed that the models with $\mathbf{c}_{opt}(\omega_1)$ exhibit a large deformation concentration to specific stories for large PGVs although $\mathbf{c}_{opt}(\omega_1)$ effectively reduces the elastic deformation responses. This tendency is seen clearly in the cases of the pulse type ground motions. On the other hand, $\mathbf{c}_{tf}$ effectively reduces both the elastic and elastic-plastic deformation responses. Moreover, $\mathbf{c}_{tf}$ effectively reduces the floor acceleration responses although $\mathbf{c}_{opt}(\omega_1)$ does not. In the cases of $\mathbf{c}_{opt}(\omega_1)$, the floor acceleration responses become large because of the occurrence of the high frequency vibration components due to the elastic higher-mode responses and the inelastic responses.

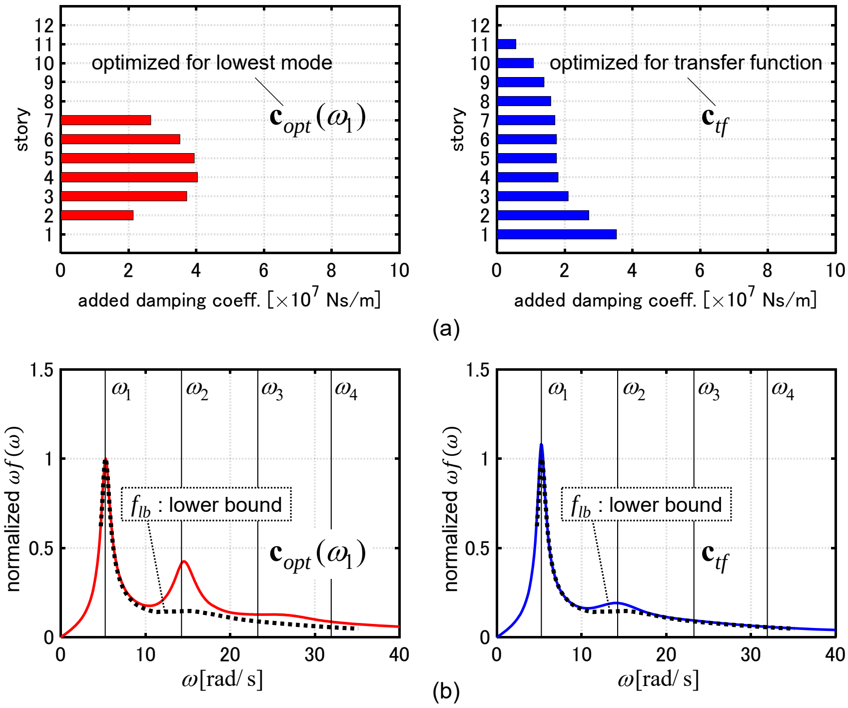

Fig. 5 Comparison of $\mathbf{c}_{opt}(\omega_1), \mathbf{c}_{tf}$ (Model 1), (a) distributions of added damping coefficients, (b) normalized sum of transfer function amplitudes of interstory velocities.

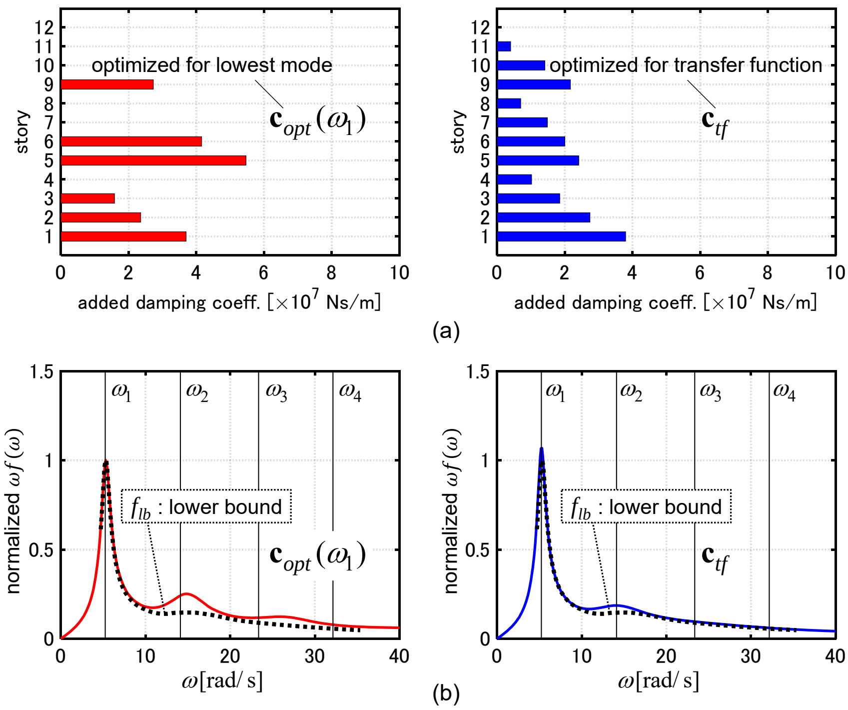

Fig. 6 Comparison of $\mathbf{c}_{opt}(\omega_1), \mathbf{c}_{tf}$ (Model 2), (a) distributions of added damping coefficients, (b) normalized sum of transfer function amplitudes of interstory velocities.

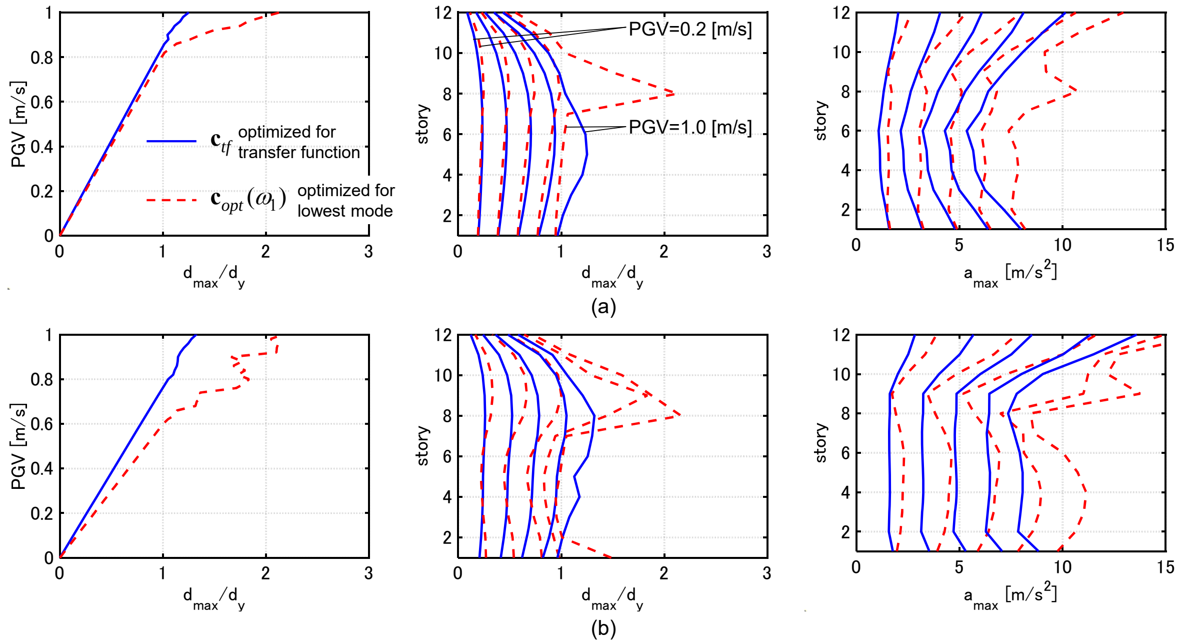

Fig. 7 IDA curves, distributions of maximum interstory drifts and distributions of maximum floor accelerations (Model 1), (a) El Centro NS component, (b) Taft EW component

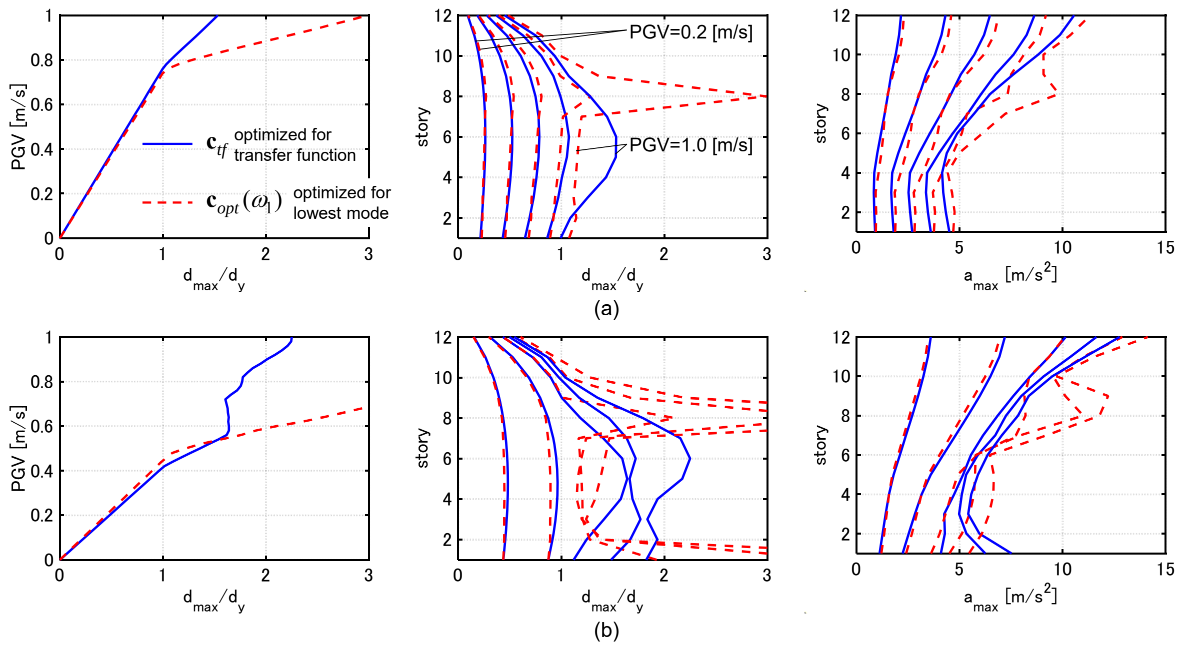

Fig. 8 IDA curves, distributions of maximum interstory drifts and distributions of maximum floor accelerations (Model 1), (a) Rinaldi Sta. FN component, (b) Kobe Univ. NS component.

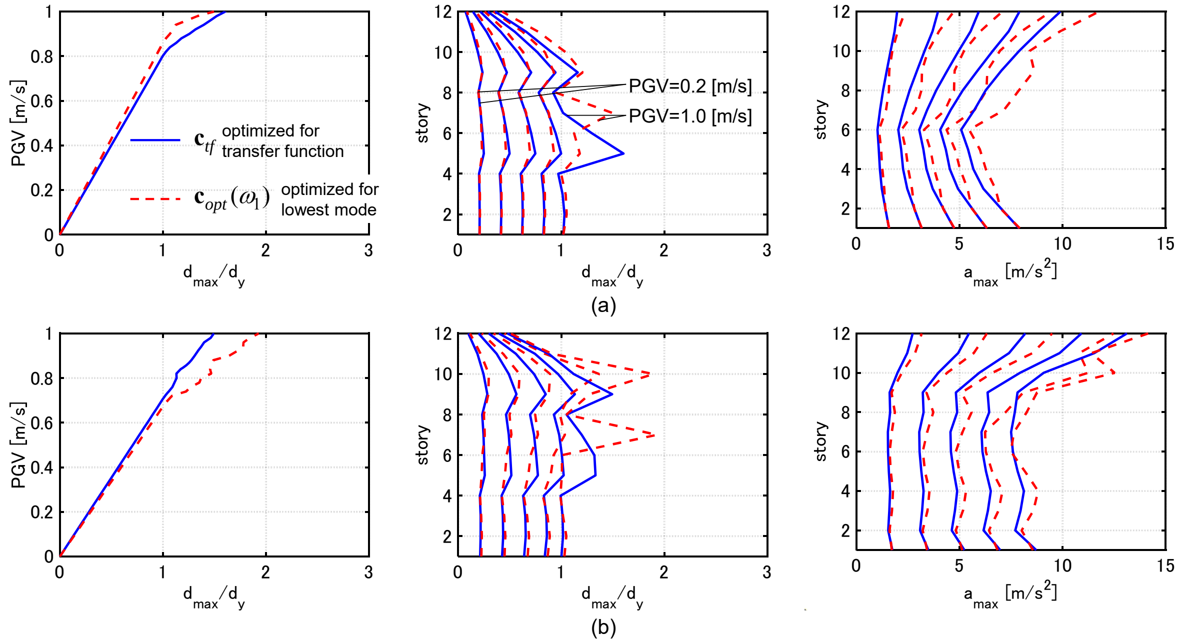

Fig. 9 IDA curves, distributions of maximum interstory drifts and distributions of maximum floor accelerations (Model 2), (a) El Centro NS component, (b) Taft EW component

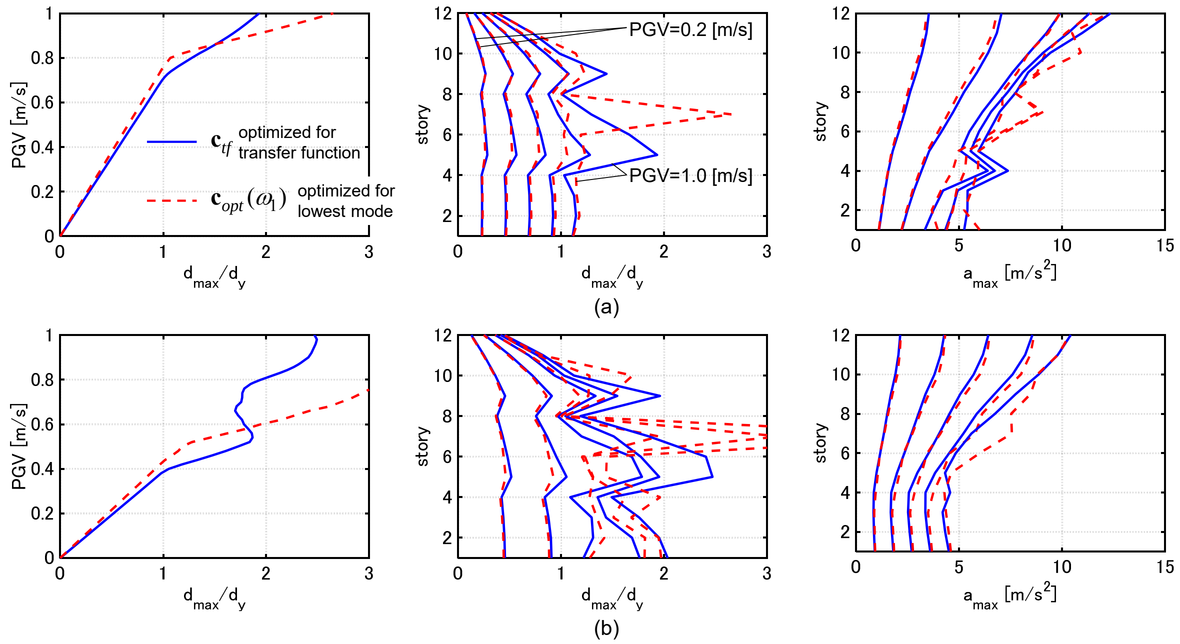

Fig. 10 IDA curves, distributions of maximum interstory drifts and distributions of maximum floor accelerations (Model 2), (a) Rinaldi Sta. FN component, (b) Kobe Univ. NS component.

4 Numerical examples for moment resisting frame

In this section, $\mathbf{c}_{opt}(\omega_1)$ and $\mathbf{c}_{tf}$ for a moment-resisting frame are compared through the transfer functions and the IDA analyses. Consider a 10-story 3-bay steel moment-resisting frame. The common story height is 4 [m], and the common span length is 7 [m]. All the floor masses are $100\times10^3\,[\mathrm{kg}]$. To consider the vertical inertial forces, $(100/6)\times10^3\,[\mathrm{kg}]$ is allocated to the top nodes of the corner columns, and $(100/3)\times10^3\,[\mathrm{kg}]$ is allocated to the top nodes of the interior columns. W21×201 and W21×182 are employed as the sections of the columns in the 1-5th stories and those in the 6-10th stories. W33×130 and W30×99 are employed as the sections of the beams in the 1-5th stories and those in the 6-10th stories. The yield stress of the beams is 240 [N/mm^2] and that of the columns is 320 [N/mm^2]. The columns are designed so as to have the large values of the plastic moment compared with those of the beams. The column bases in the 1st story are fixed. Young's modulus is set to $2.05\times10^5\,[\mathrm{N/mm^2}]$. The undamped fundamental natural period is 1.29 [s], and the structural damping ratio is 0.02 (stiffness proportional type).

The linear viscous dampers with the K-type supporting braces are treated and the dampers can be installed at all the bays in all stories. The sum of added damping coefficients has been set so that the fundamental-mode damping ratio by the dampers becomes about 0.10. It is noted that the dampers are allocated symmetrically.

The structural analysis software OpenSees is used to conduct the time-history response analysis for the elastic-plastic frame[38]. The P-delta effect of the columns and the corotational formulation of the beams are taken into account as the geometric nonlinearity. The material Steel01 with the strain hardening ratio 0.01 is applied to all the beams and the columns. The flanges of the H-shaped cross sections are modeled by 6×1 fibers, and the webs are also modeled by 6×1 fibers. All the ground motions adopted in Section 3 are used again.

The parameters in the optimization algorithms are the same as those for the shear-mass systems. The following 3-type damper placements are employed as initial designs for the search of $\mathbf{c}_{opt}(\omega_1),...,\mathbf{c}_{opt}(\omega_4)$: (i) uniform placement along height only in the center bay, (ii) uniform placement along height only in the side bays (no damper at the center bay), (iii) uniform placement along height in all the bays. As a result, the finally obtained designs have been the same for each natural frequency. $\mathbf{c}_{opt}(\omega_1)$ is employed as an initial design for the search of $\mathbf{c}_{tf}$ here again.

Figure 11 shows the distributions of the added damping coefficients of $\mathbf{c}_{opt}(\omega_1), \mathbf{c}_{tf}$, the normalized sum of the transfer function amplitudes of the interstory velocities and normalized LBTF. It can be observed that the added damping of $\mathbf{c}_{opt}(\omega_1)$ concentrates to the 2-4, 6, 7th stories, and the added dampers are placed to relatively many stories for $\mathbf{c}_{tf}$. Since the member sections switch to the smaller ones beyond the 6th story and the column bases in the 1st story are fixed, the stiffnesses of those stories are relatively large. As a result, the dampers are not allocated to those stories in the case of $\mathbf{c}_{opt}(\omega_1)$, and the dampers in those stories are relatively small in the case of $\mathbf{c}_{tf}$. It is noted that all the dampers in each floor are installed into only the center bay because the vertical deformations of the interior columns are smaller than those of the corner columns. It is pointed out that all the dampers are not always allocated to the center bay in the cases of $\mathbf{c}_{opt}(\omega_2), \mathbf{c}_{opt}(\omega_3), \mathbf{c}_{opt}(\omega_4)$ (see

Appendix). It can also be observed from Figure 11 that the transfer function amplitudes of $\mathbf{c}_{opt}(\omega_1)$ are away from LBTF near the higher-mode natural frequencies although the transfer function amplitudes are close to LBTF near ω_1. On the other hand, the transfer function amplitudes of $\mathbf{c}_{tf}$ are close to LBTF for a broader frequency range.

Figures 12, 13 present the results of the IDA analyses. It can be observed that both of $\mathbf{c}_{opt}(\omega_1)$ and $\mathbf{c}_{tf}$ effectively reduce the deformation responses under El Centro NS component, Rinaldi Sta. FN component and Kobe Univ. NS component. This results from the increase of the effectiveness of $\mathbf{c}_{opt}(\omega_1)$ for the elastic-plastic responses. The nonlinearity of the story shear-interstory drift relation of the moment resisting frame is relatively small since the plastic hinges are not formed simultaneously in all the beams on the same floor. It leads to less amplification of the higher-mode effect due to the elastic-plastic responses than that in the cases of the shear-mass systems whose story shear-interstory drift relation obeys the elastic perfectly-plastic rule. In the case of Taft EW component, $\mathbf{c}_{opt}(\omega_1)$ does not effectively reduce the deformation responses in the upper stories. Moreover, $\mathbf{c}_{tf}$ reduces the floor acceleration responses especially under the ground motions of random nature more effectively than $\mathbf{c}_{opt}(\omega_1)$. These result from the ineffectiveness of $\mathbf{c}_{opt}(\omega_1)$ for the higher modes.

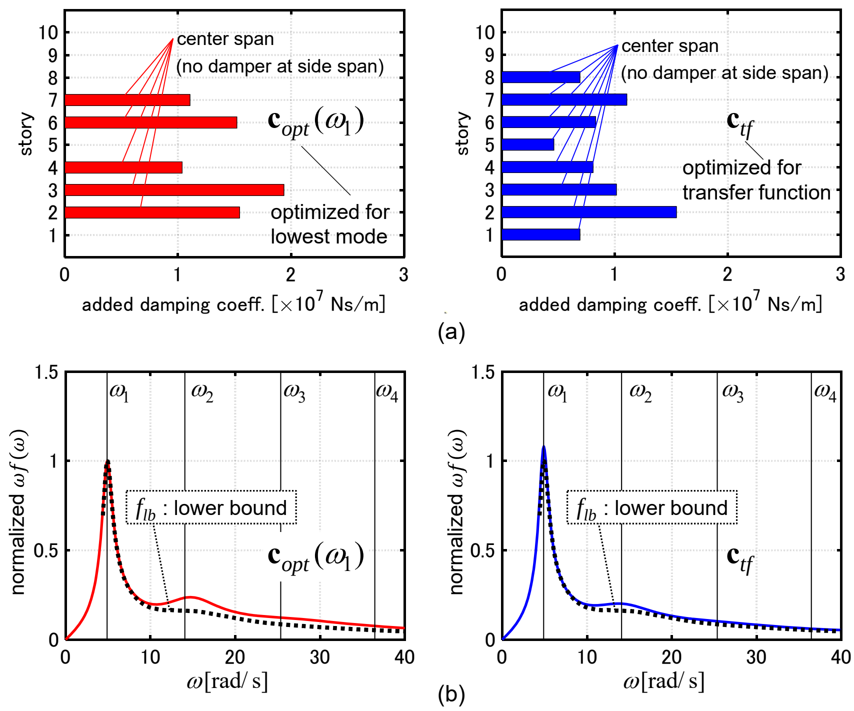

Fig. 11 Comparison of $\mathbf{c}_{opt}(\omega_1), \mathbf{c}_{tf}$ (moment-resisting frame), (a) distributions of added damping coefficients, (b) normalized sum of transfer function amplitudes of interstory velocities.

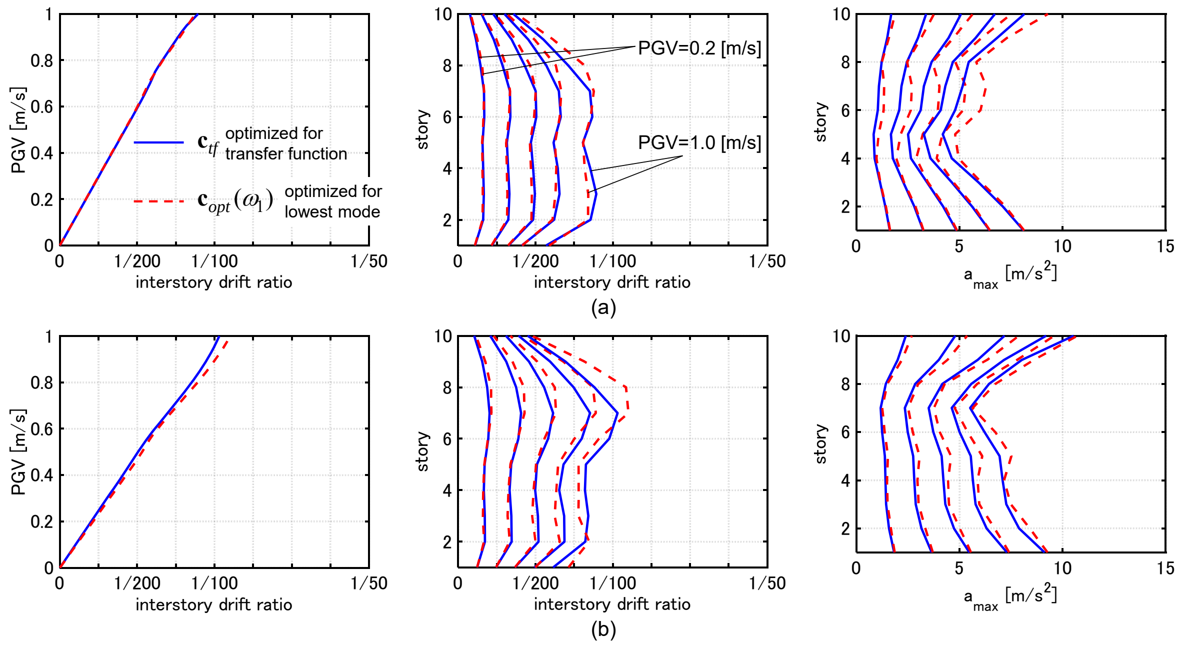

Fig. 12 IDA curves, distributions of maximum interstory drifts and distributions of maximum floor accelerations (moment-resisting frame), (a) El Centro NS component, (b) Taft EW component

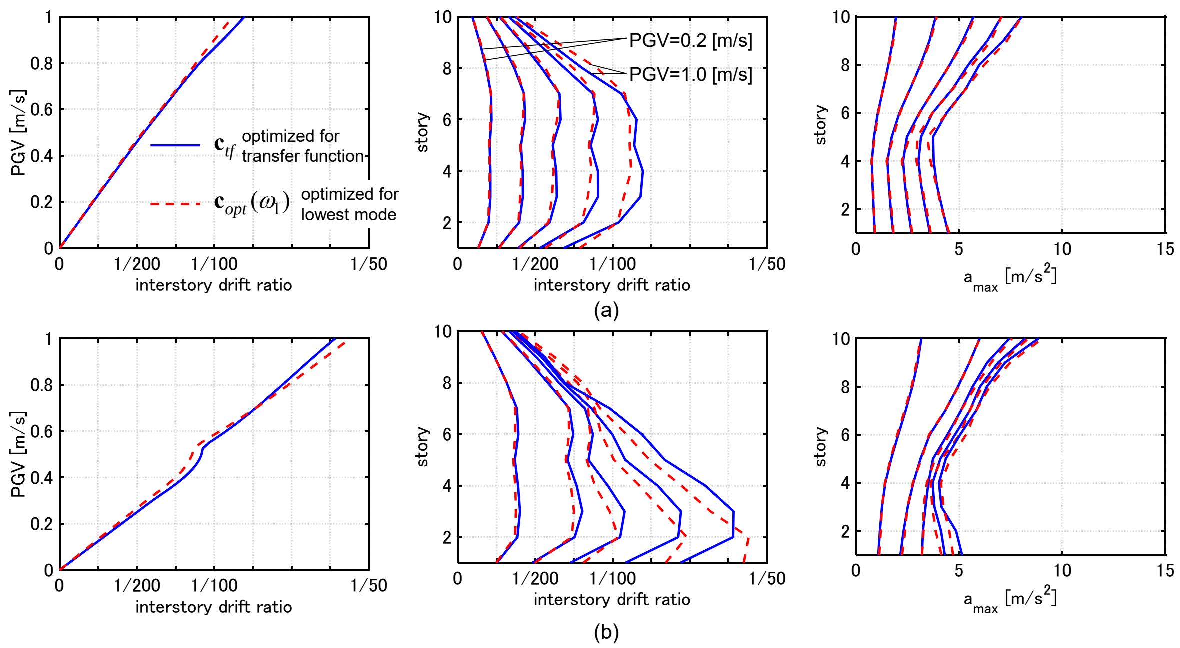

Fig. 13 IDA curves, distributions of maximum interstory drifts and distributions of maximum floor accelerations (moment-resisting frame), (a) Rinaldi Sta. FN component, (b) Kobe Univ. NS component.

5. Conclusions

A new concept of 'lower-bound transfer function (LBTF)' and a new frequency-domain optimal damper design method were presented. The main conclusions can be summarized as follows.

(1) A new concept of LBTF was proposed for visually capturing the effectiveness of damper design for each mode. LBTF expresses an ideal performance of response control in the frequency domain under the constant sum of added damping coefficients (or the total cost of dampers). When a damper design is effective for multi modes, the transfer function is plotted near the LBTF for a broader frequency range. On the contrary, when a design is not effective for some specified modes, the amplitudes of the transfer function is plotted away from the LBTF near the corresponding natural frequencies.

(2) An efficient generation method of LBTFs was presented. In the proposed method, the distribution of added damping coefficients is continuously changed so that the optimality criteria are always satisfied.

(3) An optimization problem was formulated to obtain designs with multi-modal adaptability and its solution algorithm was presented. It does not require much computational load to solve the problem since the optimization is conducted in the frequency domain and the first-order or second-order sensitivities of the objective function can be derived analytically.

(4) The proposed design $\mathbf{c}_{tf}$ for the optimized transfer function and the fundamental mode optimal damper placement $\mathbf{c}_{opt}(\omega_1)$ for shear-mass systems and moment-resisting frames were compared through the transfer functions and the IDA analyses. It was demonstrated that $\mathbf{c}_{opt}(\omega_1)$ is effective for the fundamental natural mode but not effective for the higher modes. In addition, models with $\mathbf{c}_{opt}(\omega_1)$ may exhibit large deformation concentration in specific stories for large PGV although $\mathbf{c}_{opt}(\omega_1)$ effectively reduces the elastic deformation responses. On the other hand, $\mathbf{c}_{tf}$ is effective for multi modes, and effectively reduces the floor acceleration responses and the elastic and elastic-plastic deformation responses.

(5) In the case of a moment-resisting frame, the amplification of the higher-mode effect due to the elastic-plastic responses is smaller than that in shear-mass systems whose story shear-interstory drift relation obeys the elastic perfectly-plastic rule. It leads to the increase of the effectiveness of $\mathbf{c}_{opt}(\omega_1)$ for the elastic-plastic deformation responses. Both $\mathbf{c}_{opt}(\omega_1)$ and $\mathbf{c}_{tf}$ can effectively reduce the elastic and elastic-plastic deformation responses. However, $\mathbf{c}_{opt}(\omega_1)$ is not effective for the higher modes as in the case of shear-mass systems. Therefore, $\mathbf{c}_{tf}$ reduces the floor acceleration responses more effectively than $\mathbf{c}_{opt}(\omega_1)$.

6. Acknowledgement

Part of the present work is supported by the Grant-in-Aid for Scientific Research (KAKENHI) of Japan Society for the Promotion of Science (No.18H01584, JP20J20811). This support is greatly appreciated.

7. References

1. Takewaki, I. (2009). *Building Control with Passive Dampers: -Optimal Performance-based Design for Earthquakes-*, John Wiley & Sons Ltd. (Asia).
2. Lagaros, N. D. (Ed.) (2012). *Design optimization of active and passive structural control systems*. IGI Global.
3. De Domenico, D., Ricciardi, G., and Takewaki, I. (2019). Design strategies of viscous dampers for seismic protection of building structures: A review, *Soil Dyn. Earthq. Eng*. 118, 144–165. doi: 10.1016/j.soildyn.2018. 12.024
4. Takewaki, I., and Akehashi, H. (2021). Comprehensive review of optimal and smart design of nonlinear building structures with and without passive dampers subjected to earthquake loading. *Frontiers in Built Environment*, 7, 631114.
5. Zhang, R. H., and Soong, T. T. (1992). Seismic design of viscoelastic dampers for structural applications. *J. Struct. Eng*., 118(5), 1375-1392.
6. Garcia, D.L. (2001). A simple method for the design of optimal damper configurations in MDOF structures, *Earthq. Spectra*, 17(3), 387-398.
7. Takewaki, I. (2000). An approach to stiffness-damping simultaneous optimization. *Comp. Meth. Appl. Mech.s Eng*., 189(2), 641-650.
8. Trombetti, T., and Silvestri, S. (2004). Added viscous dampers in shear-type structures: the effectiveness of mass proportional damping. *J. Earthq. Eng*., 8(02), 275-313.
9. Lavan, O., and Levy, R. (2006). Optimal design of supplemental viscous dampers for linear framed structures. *Earthq. Eng. Struct. Dyn*., 35, 337-356.
10. Cimellaro, G. P., and Retamales, R. (2007). Optimal softening and damping design for buildings. *Struct. Control Health Monit*., 14(6), 831-857.
11. Silvestri, S., Gasparini, G., and Trombetti, T. (2010). A five-step procedure for the dimensioning of viscous dampers to be inserted in building structures. *J. Earthq. Eng*., 14(3), 417-447.
12. Lavan, O., and Dargush, G.F. (2009). Multi-objective evolutionary seismic design with passive energy dissipation systems. *J. Earthq. Eng*., 13(6): 758–790.
13. Apostolakis, G., and Dargush, G. F. (2010). Optimal seismic design of moment‐resisting steel frames with hysteretic passive devices. *Earthq. Eng. Struct. Dyn*., 39(4), 355-376.
14. Yamamoto, K., Fujita, K., and Takewaki, I. (2010). H^{∞} optimization in damper placement for interstory drift control of structures. In *1st International Conference on Advances in Interaction and Multiscale Mechanics (AIMM'10) Jeju, Korea*, 321-329.
15. Whittle, J.K., Williams, M.S., Karavasilis, T.L., and Blakeborough, A. (2012). A comparison of

viscous damper placement methods for improving seismic building design, *J. Earthq. Eng*., 16(4), 540-560.

16. Sonmez, M., Aydin, E., and Karabork, T. (2013). Using an artificial bee colony algorithm for the optimal placement of viscous dampers in planar building frames. *Struct. Multidisciplinary Optimization*, 48(2), 395-409.
17. Martínez, C. A., Curadelli, O., and Compagnoni, M. E. (2014). Optimal placement of nonlinear hysteretic dampers on planar structures under seismic excitation. *Eng. Struct*., 65, pp. 89-98.
18. Pollini, N., Lavan, O., and Amir, O. (2017). Minimum‐cost optimization of nonlinear fluid viscous dampers and their supporting members for seismic retrofitting. *Earthq. Eng. Struct. Dyn*., 46(12), 1941-1961.
19. Cetin, H., Aydin, E., and Ozturk, B. (2019). Optimal Design and Distribution of Viscous Dampers for Shear Building Structures under Seismic Excitations. *Frontiers in Built Environment*, 5: 90.
20. De Domenico, D., and Ricciardi, G. (2019). Earthquake protection of structures with nonlinear viscous dampers optimized through an energy-based stochastic approach. *Eng. Struct*., 179, 523-539.
21. Aydin, E., Ozturk, B., Bogdanovic, A., and Farsangi, E. N. (2020). Influence of soil-structure interaction (SSI) on optimal design of passive damping devices. *Structures*, 28, 847-862.
22. Apostolakis, G. (2020). Optimal evolutionary seismic design of three-dimensional multistory structures with damping devices. *J. Struct. Eng*., 146(10), 04020205.
23. Marzok, A., and Lavan, O. (2021). Seismic design of multiple-rocking systems: A gradient-based optimization approach. *Earthq. Eng. Struct. Dyn*., 1–23.
24. Lavan, O., and Levy, R. (2010). Performance based optimal seismic retrofitting of yielding plane frames using added viscous damping. *Earthq. Struct*., 1(3), 307-326.
25. Akehashi, H. and Takewaki, I. (2019). Optimal Viscous Damper Placement for Elastic-Plastic MDOF Structures under Critical Double Impulse. *Frontiers in Built Environment*, 5, 20.
26. Akehashi, H., and Takewaki, I. (2020b). Simultaneous optimization of elastic-plastic building structures and viscous dampers under critical double impulse. *Frontiers in Built Environment*, 6, 211.
27. Akehashi, H., Takewaki, I. (2021b). Global optimization of hysteretic dampers for elastic-plastic MDOF structures via hybrid approach of real-coded genetic algorithm and local search. *J. Struct. Construct. Eng*., 86(787), 1335–1344 (in Japanese). DOI 10.3130/aijs.86.1335.
28. Attard, T. L. (2007). Controlling all interstory displacements in highly nonlinear steel buildings using optimal viscous damping. *J. Struct. Eng*., 133(9), 1331-1340.
29. Akehashi, H. and Takewaki, I. (2021c). Ideal drift response curve for robust optimal damper design for elastic-plastic MDOF structures under multi-level earthquakes. *Comp. Modeling Eng. Sciences*.

DOI 10.32604/cmes.2021.017204.

30. Takewaki, I. (1997). Optimal Damper Placement for Minimum Transfer Functions, *Earthq. Eng. Struct. Dyn.*, 26(11), 1113-1124.
31. Aydin, E., Boduroglub, M.H., and Guney, D. (2007). Optimal damper distribution for seismic rehabilitation of planar building structures. *Eng. Struct*., 29, 176-185.
32. Akehashi, H. and Takewaki, I. (2020a). Comparative investigation on optimal viscous damper placement for elastic-plastic MDOF structures: Transfer function amplitude or double impulse. *Soil Dyn. Earthq. Eng.*, 130, 105987.
33. Rodriguez, M. E., Restrepo, J. I. and Carr, A. J. (2002). Earthquake-induced floor horizontal accelerations in buildings. *Earthq. Eng. Struct. Dyn.*, 31, 693-718.
34. Hutt, C. M., Almufti, I., Willford, M., and Deierlein, G. (2016). Seismic loss and downtime assessment of existing tall steel-framed buildings and strategies for increased resilience. *J. Struct. Eng*., 142(8), C4015005.
35. Vukobratović, V., and Fajfar, P. (2016). A method for the direct estimation of floor acceleration spectra for elastic and inelastic MDOF structures. *Earthq. Eng. Struct. Dyn*., 45(15), 2495-2511.
36. Akehashi, H., Takewaki, I. (2021a). Modeling of resilience based on categorized recovery scenario and improving resilience with viscous damper. *J. Struct. Construct. Eng*., 86(782), 577–588 (in Japanese). DOI 10.3130/aijs.86.577.
37. Vamvatsikos, D., and Cornell, C.A. (2001). Incremental dynamic analysis. *Earthq. Eng. Struc.t Dyn.*, 31(3), 491–514.
38. McKenna, F. (2011). OpenSees: a framework for earthquake engineering simulation. *Computing Science Eng*., 13(4), 58-66.

Appendix

Figures A1, A2 illustrates the distributions of the added damping coefficients of $\mathbf{c}_{opt}(\omega_2), \mathbf{c}_{opt}(\omega_3), \mathbf{c}_{opt}(\omega_4)$ and the corresponding normalized transfer function amplitudes for Model 1, 2 (shear-mass system). Normalized LBTFs are also plotted. Figure A3 shows those for the moment-resisting frame. It can be observed that the transfer function amplitudes are close to LBTFs near the corresponding natural circular frequencies. Unlike the case of $\mathbf{c}_{opt}(\omega_1)$, the dampers are allocated into not only the center bay but also the side bays for the moment-resisting frame. In other words, the vertical displacements of the nodes (outer nodes) do not always decrease the effectiveness of the dampers in the cases of the higher modes. The allocation of the dampers into the side bays may be more effective than the allocation into the center bay due to the relation between the directions of the lateral displacements and that of the vertical displacements of the nodes.

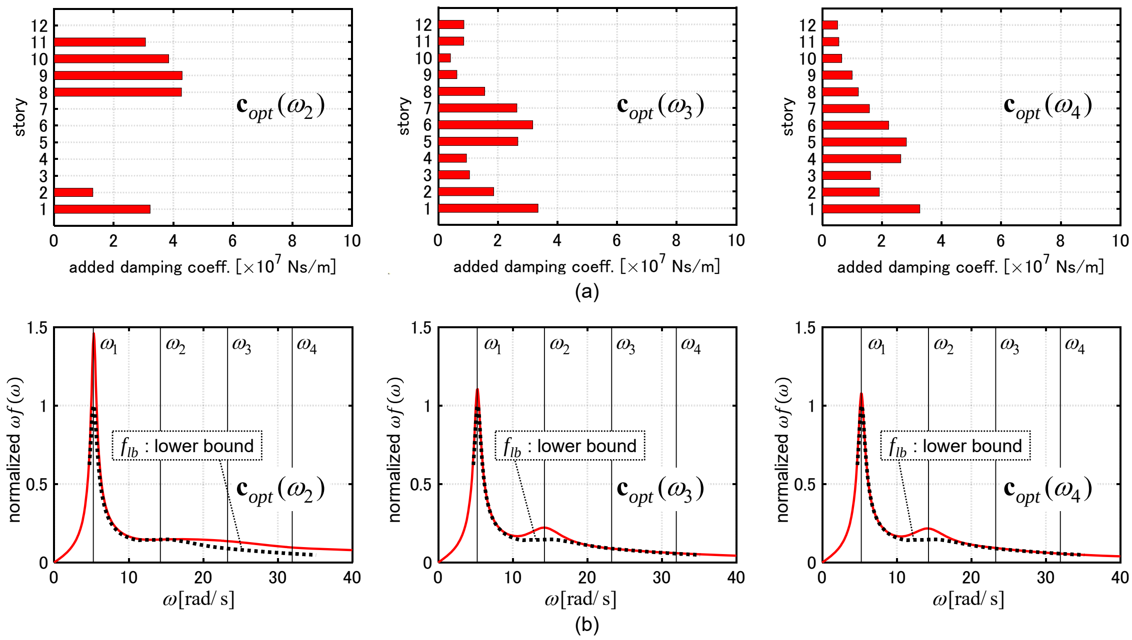

Fig. A1 Comparison of $\mathbf{c}_{opt}(\omega_2), \mathbf{c}_{opt}(\omega_3), \mathbf{c}_{opt}(\omega_4)$ (Model 1), (a) distributions of added damping coefficients, (b) normalized sum of transfer function amplitudes of interstory velocities.

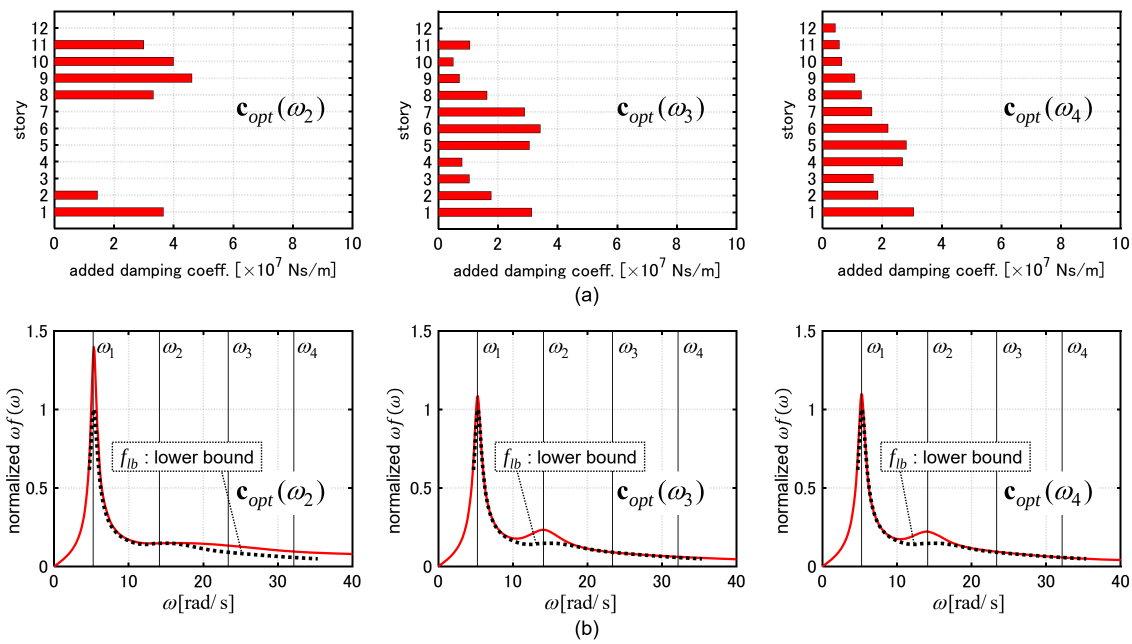

Fig. A2 Comparison of $\mathbf{c}_{opt}(\omega_2), \mathbf{c}_{opt}(\omega_3), \mathbf{c}_{opt}(\omega_4)$ (Model 2), (a) distributions of added damping coefficients, (b) normalized sum of transfer function amplitudes of interstory velocities.

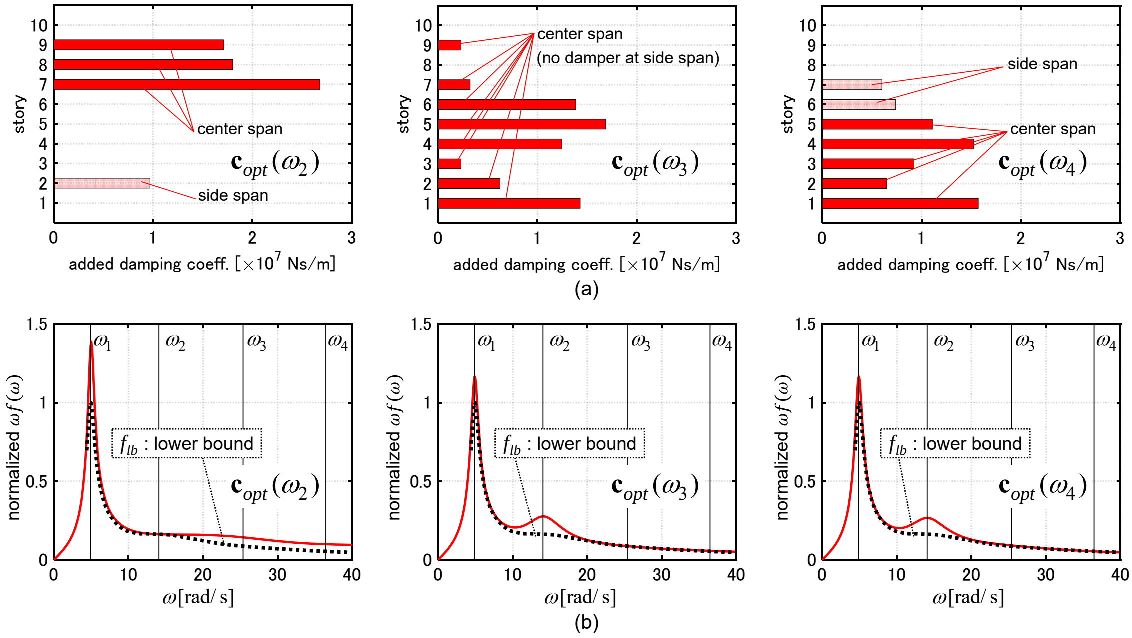

Fig. A3 Comparison of $\mathbf{c}_{opt}(\omega_2), \mathbf{c}_{opt}(\omega_3), \mathbf{c}_{opt}(\omega_4)$ (moment resisting frame), (a) distributions of added damping coefficients, (b) normalized sum of transfer function amplitudes of interstory velocities.